35th Annual International Conference of the IEEE EMBS
Osaka, Japan, 3 - 7 July, 2013

Computational Assessment of the Fractional Flow Reserve from Intravascular Ultrasound and Coronary Angiography Data: a Pilot Study

Panagiotis K. Siogkas, Michail I. Papafaklis, Antonis I. Sakellarios, Kostas A. Stefanou, Christos V. Bourantas, Lambros M. Athanasiou, Christos V. Bellos, Themis P. Exarchos, Katerina K. Naka Lampros K. Michalis, Oberdan Parodi and Dimitrios I. Fotiadis, *Senior IEEE Member*

***Abstract*— Cardiovascular disease is one of the primary causes of morbidity and mortality around the globe. Thus, the diagnosis of critical lesions in coronary arteries is of utmost importance in clinical practice. One useful and efficient method to assess the functional severity of one or multiple lesions in a coronary artery is the calculation of the fractional flow reserve (FFR). In the current work, we present a method which allows the calculation of the FFR value computationally, without the use of a pressure wire and the induction of hyperemia, using intravascular ultrasound (IVUS) and biplane angiography images for three-dimensional (3D) coronary artery reconstruction and measurements of the volumetric flow rate derived from angiographic sequences. The simulated FFR values were compared to the invasively measured FFR values in 7 cases, presenting high correlation (r=0.85) and good agreement (mean difference=0.002). FFR assessment without employing a pressure wire and the induction of hyperemia is feasible using 3D reconstructed coronary artery models from angiographic and IVUS data coupled with computational fluid dynamics.**

I. Introduction

Coronary Artery Disease (CAD) is the most prevalent cause of death in patients suffering from cardiovascular diseases. The traditional coronary angiography examination provides a visual insight into the severity of existing stenoses on the coronary vasculature of a patient. However, several lesions might be of high risk, even though anatomically, might seem harmless. One method to assess the functional severity of such lesions is the measurement of the FFR value. In a stenosed coronary vessel, the maximal coronary flow in the stenosed artery divided by the maximal coronary flow in the same artery without the stenosis equals the FFR value. If hyperemia is induced, myocardial resistances remain constant and the central venous pressure is neglected, allowing the measurement of the myocardial Fractional Flow Reserve (FFR_{myo}) which is defined as the pressure distal to the stenosis (P_r) divided by the aortic pressure (P_e) as it is shown in Eq.(1) [1].

$$FFR_{myo} = \frac{P_r}{P_e}, \quad (1)$$

Fig.1 represents the rationale of the FFR measurement procedure [1]. The FFR score has a cut-off value of 0.75-0.80, below which ischemia is detected.

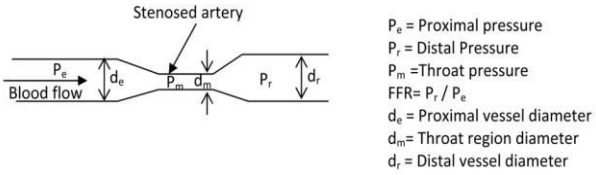

Fig. 1: Representation of a stenosed arterial segment. The proximal and distal pressure values (P_e and P_r) are measured with a pressure wire. Reproduced from Govindarajua, et al. [1], with permission from Elsevier.

Thus, the calculation of hemodynamic parameters such as pressure values within the artery and consequently FFR values is extremely important in clinical practice.

Computational fluid dynamics (CFD) techniques can provide the *in vivo* calculation of hemodynamic factors including the distribution of pressure and endothelial shear stress along the length of coronay arteries. However, realistic three-dimensional (3D) coronary artery reconstruction is critical for accurate assessment. Several 3D reconstruction methods have been published regarding the coronary vasculature. The fusion of two imaging techniques is often required to achieve a geometrically-accurate result which incorporates the complex 3D geometry of coronary arteries on the epicardial surface and the detailed lumen and wall morphology. The most common hybrid methods of imaging techniques include intravascular ultrasound (IVUS) and biplane coronary angiography images [2-3], IVUS and CT

This work is part funded by the European Commission (Project ARTREAT: Multi-level patient-specific artery and atherogenesis model for outcome prediction, decision support treatment, and virtual hand-on training, FP7-224297).

P.K. Siogkas, A.I. Sakellarios, C.V Bellos, L.M Athanasiou and D.I. Fotiadis are with the Unit of Medical Technology and Intelligent Information Systems, Dept. of Materials Science and Engineering, University of Ioannina, GR 45110 (email: psiogkas@cc.uoi.gr, ansakel@cc.uoi.gr, cbellos@cc.uoi.gr ,lmathanas@cc.uoi.gr, corresponding author phone: +302651008803; fax: +302651008889; e-mail: fotiadis@cs.uoi.gr).

M.I Papafaklis is with the Cardiovascular Division, Brigham and Women's Hospital, Harvard Medical School, Boston, MA 02115, USA (email: m.papafaklis@yahoo.com).

C.V Bourantas is with the Dept. of Cardiology, Academic Unit, University of Hull, HU16 5JQ, Kingston-upon-Hull, United Kingdom.

K.A Stefanou and T.P. Exarchos are researchers in Biomedical Research Institute – FORTH, GR 45110 Ioannina, Greece (email: kstefan@cc.uoi.gr, exarchos@cc.uoi.gr).

K.K. Naka and L.K. Michalis are with the Michaelideion Cardiac Center, Dept. of Cardiology in Medical School, University of Ioannina, GR 45110 Ioannina, Greece (email: anaka@cc.uoi.gr, lmihalis@cc.uoi.gr).

O. Parodi is with the Instituto di Fisiologia Clinica, Consiglio Nazionale delle Ricerche (IFC CNR), Pisa, Italy.

angiography images [4] and Optical Coherence Tomography (OCT) combined with biplane angiography [5]. Using the 3D reconstructed models, CFD simulations have been carried out under the assumption that the deformation of the arterial wall is present (Fluid Structure Interaction models) or not present (Rigid Wall assumption) [6-21]. The rigid wall simulations are executed in a shorter time period, whereas the Fluid Structure Interaction (FSI) simulations are more accurate but require more time and computational resources due to the large number of equations that need to be solved.

In the current work, we present a method that allows the calculation of the FFR values in 3D coronary arterial models, reconstructed from IVUS and coronary angiographic images without the induction of hyperemia, and we compare the FFR estimations to the actual FFR values measured invasively using a pressure wire. The key aspect of the proposed method lies on the fact that the use of the pressure wire is not required since routine data from the angiography sequence and aortic pressure during diagnostic catheterization are used for estimating the appropriate boundary conditions for the simulation. Thus, FFR assessment using our method does not require a pressure wire and the induction of hyperemia, and thus it is cost effective. Moreover, it provides the opportunity of retrospective FFR assessment after the completion of the catheterization.

II. Materials and Methods

A. Dataset

In this report, seven coronary arterial segments (4 right coronary arteries [RCA] and 3 left anterior descending arteries [LAD]) were studied in 6 patients that underwent angiography and IVUS examination. Pressure values were obtained at a distal artery location of interest (i.e., distal to a stenosis visible in angiography) using a coronary guide wire with miniaturized transducers at the tip of the wire (Combo wire, Volcano Corp., San Diego, CA). The examined segments were mildly diseased, presenting FFR values ranging between 0.92-0.99. Only one patient presented angina, a fact that constitutes a limitation in our study and will be presented in detail in the last section.

B. 3D Reconstruction of the Arterial Segments

The 3D reconstruction process consists of several steps and has been previously presented and validated by our group [2]. In brief, the catheter path is identified in the biplane end-diastolic angiographic images, and the 3D catheter path is extracted. Then, the end-diastolic frames are identified and extracted from the IVUS sequence. The lumen borders are segmented from the end-diastolic images and placed onto the 3D catheter path. Finally, the IVUS contours are appropriately orientated using efficient 3D geometry algorithms, and the orientation of the first IVUS frame is determined so that the 3D model matches the silhouette of the lumen in the biplane angiographic images.

C. Flow measurement

A key feature of the presented method is the calculation of the volumetric flow rate (average flow during the cardiac cycle) under resting conditions from the angiographic image sequence. The flow rate is calculated by the angiographic frames required for the radio-opaque contrast material to pass from the inlet to the outlet of the studied segment, the corresponding volume directly computed from the 3D reconstructed coronary segment and the frame rate. A representative case with the flow calculation is presented in Fig. 2. The final equation that is used to calculate the flow rate is the following [22]:

$$\text{Flow Rate} = \frac{\text{Frame rate}(\text{frames}/\text{sec}) \times \text{3D volume}(\text{ml})}{\text{Frame count}}, \quad (2)$$

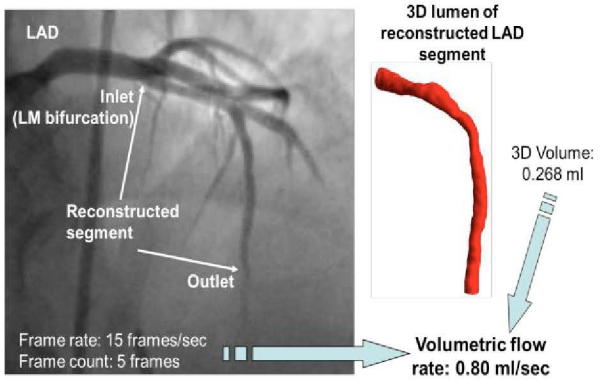

Fig. 2: Flow rate measurement procedure.

D. Blood Flow simulations

Steady state blood flow simulations were carried out on the 3D models assuming that the arterial wall is rigid.

a) Fluid Dynamics

Blood flow is modeled using the Navier-Stokes and the continuity equations:

$$\rho\frac{\partial \mathbf{v}}{\partial t} + \rho(\mathbf{v}\bullet\nabla)\mathbf{v} - \nabla\bullet\boldsymbol{\tau} = 0, \quad (3)$$

$$\nabla\bullet(\rho\mathbf{v}) = 0, \quad (4)$$

where $\mathbf{v}$ is the blood velocity vector and $\boldsymbol{\tau}$ is the stress tensor, defined as:

$$\boldsymbol{\tau} = -p\delta_{ij} + 2\mu\varepsilon_{ij}, \quad (5)$$

where δ_{ij} is the Kronecker delta, μ is the blood dynamic viscosity, p is the blood pressure and ε_{ij} is the strain tensor calculated as:

$$\varepsilon_{ij} = \frac{1}{2}\left(\nabla\mathbf{v} + \nabla\mathbf{v}^T\right). \quad (6)$$

Blood was treated as a Newtonian fluid having density 1050 kg/m^3 and dynamic viscosity 0.0035 Pa·s and blood flow was considered to be laminar and incompressible.

b) Boundary Conditions

The average patient-specific aortic pressure under resting conditions was applied at the inlet, while at the outlet the average coronary blood flow under resting conditions in the diastolic wave-free period (derived from the iFR paradigm [23]) of the cardiac cycle was determined and applied. The wave-free period in diastole begins 25% of the way into diastole and ends 5 ms before the end of diastole. Fig. 3 presents the wave-free period in a generic flow waveform. The average coronary blood flow during the diastolic wave-free period was determined using the average patient-specific volumetric flow rate throughout the cardiac cycle (as described above) and a generic coronary flow waveform for all patients. At the wall of the artery, no-slip boundary condition was imposed.

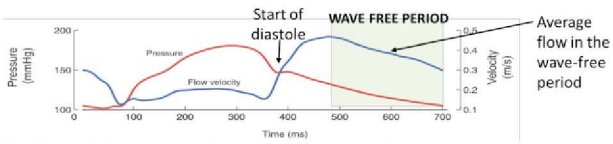

Fig. 3: Fig. 3: Pressure and flow waveforms during the cardiac cycle; the wave-free period in diastole is denoted. Adapted from Sen, et al. [23], with permission from Elsevier.

c) Mesh

The generated 3D models were discretized into tetrahedral elements with a mesh density of approximately 3,000 elements per mm^3. The mesh density was determined after a mesh sensitivity analysis was performed.

III. Results

The objective of the presented work was to investigate the efficiency of the proposed FFR calculation method in a dataset of 7 patient-specific coronary arterial segments. Linear regression analysis and the Bland-Altman plot were performed to investigate the correlation and agreement between the simulated and the actual FFR values. Fig. 4 illustrates a representative example of an LAD segment (corresponding to the angiographic images in Fig. 2) with the simulated FFR (sFFR) assessment along the length of the artery; sFFR at the outlet was 0.92, while the invasively measured FFR value was 0.94.

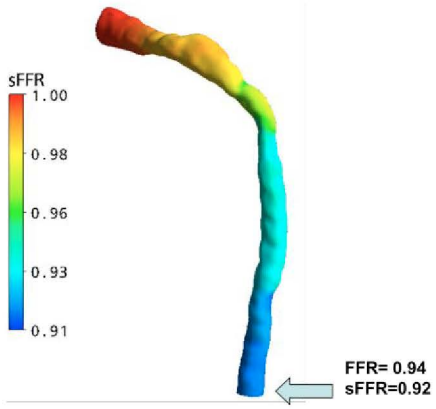

Fig. 6: Simulated FFR distribution throughout a LCA segment and comparison to the measured FFR value.

The linear regression analysis showed a good correlation between the sFFR and the actual FFR values with an r value of 0.85. The regression analysis is shown in detail in Fig. 5.

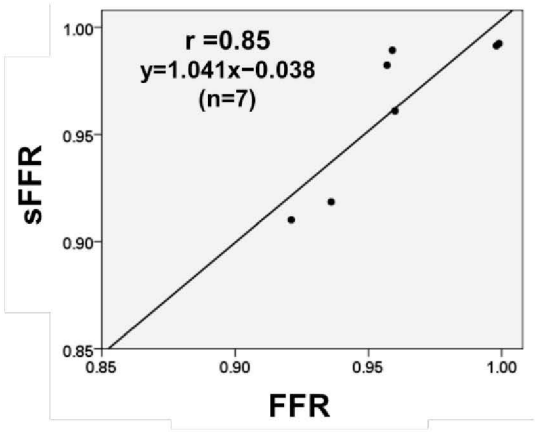

Fig. 4: Linear Regression Analysis for all 7 cases.

The Bland-Altman plot demonstrated a high similarity between the calculated and the invasively measured FFR values with a mean difference of 0.002 between the sFFR estimations and the invasively measured FFR. The Bland-Altman plot is presented in Fig. 6.

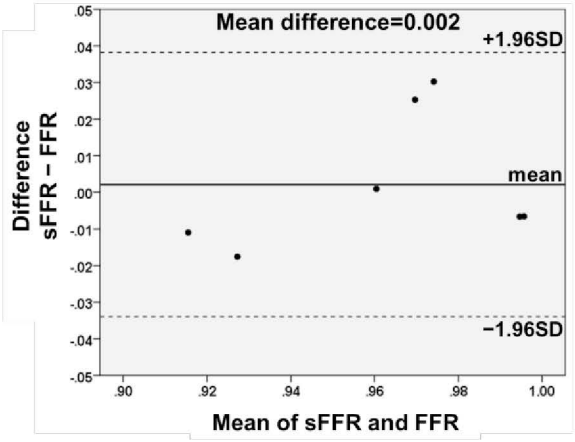

Fig. 5: Bland-Altman plot for all 7 cases.

IV. Discussion

In the current study, we proposed a method which enables FFR assessment in 3D coronary arterial models reconstructed from IVUS and angiographic images without the use of a pressure wire, and we validated our approach by comparing the sFFR values to the FFR values that were measured conventionally using a pressure wire. Arterial segments from 6 patients with mild lesions were included in this pilot study. The results that were obtained with the proposed method correlated very well to the invasively measured FFR values, indicating the efficiency of our method. Moreover, one main advantage is that the simulated FFR values are obtained without the induction of hyperemia. Another key element of our study is the fact that our method can be considered as semi-invasive whereas the traditional FFR measurement method is fully invasive since it requires the insertion of a wire in the coronary artery. Of note, our

approach could provide a cost effective method for measuring FFR since the use of costly materials/drugs (i.e., pressure wire and adenosine) is not required. Finally, our method also enables FFR assessment using retrospective data after the completion of the catheterization if the appropriate data are available. Future work will be focused on the 3D reconstruction of coronary segments using only biplane angiographic images, which in combination with the current methodology, will constitute a powerful tool for the calculation of the FFR value using only routine angiographic data.

Our study is limited by the small number of cases included. Furthermore, all cases presented only mild lesions with FFR values from 0.92-0.99, values that belong to the upper normal range which is above the 0.75-0.80 cut-off value which indicates the absence/presence of inducible ischemia. Finally, our method does not allow the reconstruction of side branches, and thus, their effect on blood flow is not incorporated.

V. CONCLUSIONS

Our proof-of-concept pilot study demonstrated that FFR assessment using 3D reconstructed coronary models from angiographic/IVUS data and computational fluid dynamics is feasible, and it does not require neither the use of a pressure wire nor the induction of hyperemia. Large studies are necessary to prove the efficacy of this approach in the clinical setting. This method is expected to facilitate and broaden the measurement of FFR in patients undergoing cardiac catheterization.

REFERENCES

[1] K. Govindarajua, I.A. Badruddina, G. N. Viswanathanb, *et al*., "Evaluation of functional severity of coronary artery disease and fluid dynamics' influence on hemodynamic parameters: A review," *Physica Medica,* in press, 2012, doi:10.1016/j.ejmp.2012.03.008.

[2] C.V. Bourantas, I. C. Kourtis, M.E. Plissiti, *et al*., "A method for 3D reconstruction of coronary arteries using biplane angiography and intravascular ultrasound images," *Computerized Medical Imaging and Graphics*, vol. 29(8), pp. 597-606, 2005.

[3] C.V. Bourantas, F.G. Kalatzis, M.I. Papafaklis, *et al.,* "ANGIOCARE: an automated system for fast three dimensional coronary reconstruction using angiographic and intracoronary ultrasound data," *Catheterization and Cardiovascular Interventions*, vol. 72(2), pp. 166-75, 2008.

[4] A.G. van der Giessen, M. Schaap, F.J. Gijsen, *et al.,* "3D fusion of intravascular ultrasound and coronary computed tomography for in-vivo wall shear stress analysis: a feasibility study," *International Journal of Cardiovascular Imaging*, vol. 26(7), pp. 781-796, 2010.

[5] L.M. Athanasiou, C.V. Bourantas, P.K. Siogkas, *et al*., "3D reconstruction of coronary arteries using Frequency Domain Optical Coherence Tomography images and biplane angiography," *Conf Proc IEEE Eng Med Biol Soc*, vol. 2012, pp. 2647-50, 2012.

[6] F. Kabinejadian, D.N. Ghista, "Compliant model of a coupled sequential coronary arterial bypass graft: Effects of vessel wall elasticity and non-Newtonian rheology on blood flow regime and hemodynamic parameters distribution," *Medical Engineering & Phys* 34(7):860-872, 2012.

[7] M. Malve, A. Garcia, J. Ohayon, *et al.,* "Unsteady blood flow and mass transfer of a human left coronary artery bifurcation: FSI vs. CFD," *International Communications in Heat and Mass Transfer,* vol. 39(6), pp. 745-751, 2012.

[8] P. Vasava, P. Jalali, M. Dabagh, *et al*., "Finite Element Modelling of Pulsatile Blood Flow in Idealized Model of Human Aortic Arch: Study of Hypotension and Hypertension," *Computational and Mathematical Methods in Medicine*, vol. 2012, Article ID 861837, 14 pages, 2012.

[9] Md. A. Ikbala, S. Chakravartya, Sarifuddin, *et al.,* "Unsteady Analysis of Viscoelastic Blood Flow through Arterial Stenosis," *Chemical Engineering Communications,* vol. 199(1), pp. 40-62, 2012.

[10] J.R. Leach, V.L. Rayz, M.R.K. Mofrad, *et al.* "An efficient two-stage approach for image-based FSI analysis of atherosclerotic arteries." *Biomechanics and Modeling in Mechanobiology,* vol. 9(2), pp. 213-223, 2010.

[11] D. Bluestein, Y. Alemu, I. Avrahami, *et al.*, "Influence of microcalcifications on vulnerable plaque mechanics using FSI modeling," *Journal of Biomechanics*, vol. 41, pp. 1111–1118, 2008.

[12] S.A. Kock, J.V. Nygaard, N. Eldrup, *et al.*, "Mechanical stresses in carotid plaques using MRI-based fluid-structure interaction models," *Journal of Biomechanics,* vol. 41(8), pp. 1651-1658, 2008.

[13] A. Borghi, N.B. Wood, R.H. Mohiaddin, *et al.*, "Fluid-solid interaction simulation of flow and stress pattern in thoracoabdominal aneurysms: A patient-specific study," *Journal of Fluids and Structures*, vol. 24(2), pp. 270-280, 2008.

[14] R. Torii, M. Oshima, T. Kobayashi, *et al.*, "Fluid-structure interaction modeling of a patient-specific cerebral aneurysm: influence of structural modeling," *Computational Mechanics*, vol. 43(1), pp. 151-159, 2008.

[15] M.X. Li, J.J. Beech-Brandt, L.R. John, *et al.*, "Numerical analysis of pulsatile blood flow and vessel wall mechanics in different degrees of stenoses," *Journal of Biomechanics*, vol. 40(16), pp. 3715-3724, 2007.

[16] B. Vahidi, and N. Fatouraee, "Large deforming buoyant embolus passing through a stenotic common carotid artery: A computational simulation," *Journal of Biomechanics*, vol. 45(7), pp. 1312-1322, 2012.

[17] S.H. Lee, H.G. Choi, and J.Y. Yoo*,* "Finite element simulation of blood flow in a flexible carotid artery bifurcation," *Journal of Mechanical Science and Technology*, vol. 26(5), pp. 1355-1361, 2012.

[18] X.H. Wang, and X.Y. Li, "Fluid-structure interaction based study on the physiological factors affecting the behaviors of stented and non-stented thoracic aortic aneurysms," *Journal of Biomechanics*, vol. 44(12), pp. 2177-2184, 2011.

[19] J. Lantz, J. Renner, and Karlsson M., "Wall Shear Stress in a Subject Specific Human Aorta - Influence of Fluid-Structure Interaction," *International Journal of Applied Mechanics*, vol. 3(4), pp. 759-778, 2011.

[20] V. Vavourakis, Y. Papaharilaou, and J.A. Ekaterinaris*,* "Coupled fluid-structure interaction hemodynamics in a zero-pressure state corrected arterial geometry," *Journal of Biomechanics*, vol. 44(13), pp. 2453-2460, 2011.

[21] E.O. Kung, A.S. Les, C.A. Figueroa, *et al.*, "In Vitro Validation of Finite Element Analysis of Blood Flow in Deformable Models," *Annals of Biomedical Engineering* 39(7): 1947-1960, 2011.

[22] P.H. Stone, A.U. Coskun, S. Kinlay, *et al.*, "Effect of endothelial shear stress on the progression of coronary artery disease, vascular Remodeling, and in-stent restenosis in humans: in vivo 6-month follow-up study," *Circulation*, vol. 108, pp. 438-444, 2003.

[23] S. Sen, J. Escaned, I.S. Malik, *et al.*, "Development and Validation of a New Adenosine-Independent Index of Stenosis Severity From Coronary Wave–Intensity Analysis," *Journal of the American College of Cardiol*ogy, vol. 59(15), pp.1392-1402, 2012.